sciendo

Transport and Telecommunication, 2025, volume 26, no. 3, 292-301
Transport and Telecommunication Institute, Lauvas 2, Riga, LV-1019, Latvia
DOI 10.2478/ttj-2025-0022

DISTORTION COMPENSATION IN MULTI-CAMERA SYSTEMS WITH WIDE-ANGLE OPTICS FOR "SMART HELMET" APPLICATIONS

Alexander Grakovski[1], Nikita Ostrovenec[2], Ivan Gercev[3], Alexander Krainukov[4], Vladimir Petrov[5], Emmanuel Merchan[6], Samuel Moveh[7], Oleksandr Pasha[8], Reinis Tocelovskis[9]

[1-7]Transport and Telecommunication Institute
Riga, Latvia, 2 Lauvas str.
[1]avg@tsi.lv, [2]nikita.o@inbox.lv, [3]gercevs.i@tsi.lv,
[4]krainukovs.a@tsi.lv, [5]petrovs.v@tsi.lv, [6]merchan.e@tsi.lv, [7]moveh.s@tsi.lv
[8-9]3D Engineering SIA
Liepaja, Latvia, 41-33 Mežu str.
[8]oleksandr@3d-engineering.eu, [9]reinis@3d-engineering.eu

This paper presents a distortion compensation algorithm for multi-camera systems that does not require specialized calibration targets. A review of classical distortion models as well as modern calibration approaches (such as OpenCV) is provided. A modification of the distortion compensation algorithm is proposed, and an experimental comparison with the classical Brown–Conrady model is conducted using data from cameras equipped with the Sony IMX462 sensor. The results show that the proposed algorithm achieves projection rectification comparable to target-based calibration while preserving a wide field of view. This opens up opportunities for applying the method in wearable monitoring systems, panoramic image creation, and pipeline inspection, where the use of calibration targets is challenging.

Keywords: Panoramic imaging, multi-camera system, fish-eye lens, radial distortion, camera calibration, distortion compensation

1. Introduction

In recent years, the concept of a "smart helmet", as a wearable device equipped with several synchronized cameras, has attracted significant attention as a tool for rapid monitoring of transportation infrastructure, underground utilities, and extended pipelines (Kim and Choi, 2022).

The placement of four miniature cameras around the perimeter (Figure 1) provides a complete 360° horizontal field of view, however, it also introduces a number of real-time computer vision challenges, including geometric synchronization of channels, correction of optical distortion, and subsequent stitching of frames into a single panorama.

The problem of barrel distortion from wide-angle and fish-eye lenses is particularly acute: at a field of view of approximately 141° (as in the Sony IMX462 module), straight scene lines become curved, which disrupts descriptor correlation and leads to breaks at image seams (Zhang *et al*., 2023; Yin *et al.*, 2024).

Existing multi-parameter models of Brown–Conrady and Kannala–Brandt straighten lines effectively, but crop the image periphery, reducing the useful field of view to 80–90%. For wearable systems, such loss of coverage is critical: the operator is deprived of information from side sectors where obstacles or pipe defects may be present.

The *goal* of this research is to develop a simple single-parameter algorithm for radial distortion compensation that:

- preserves the original field of view;
- ensures residual line curvature below 1%;
- requires minimal computational resources and is suitable for implementation on a server (dock station) or on the helmet's embedded GPU.

The proposed modification of the radial correction function resolves the "accuracy ↔ field of view (FOV)" trade-off and can be easily integrated into a standard image stitching pipeline (Xian *et al.,* 2023), making it technologically attractive for *Smart Helmet*-class systems.

2. Causes, classification, and models of distortion

Geometric distortion is one of the fundamental problems in optical systems, arising from the imperfections of the real lens design compared to the idealized “thin lens” model (Brown, 1971). The main causes of distortion can be divided into several key categories.

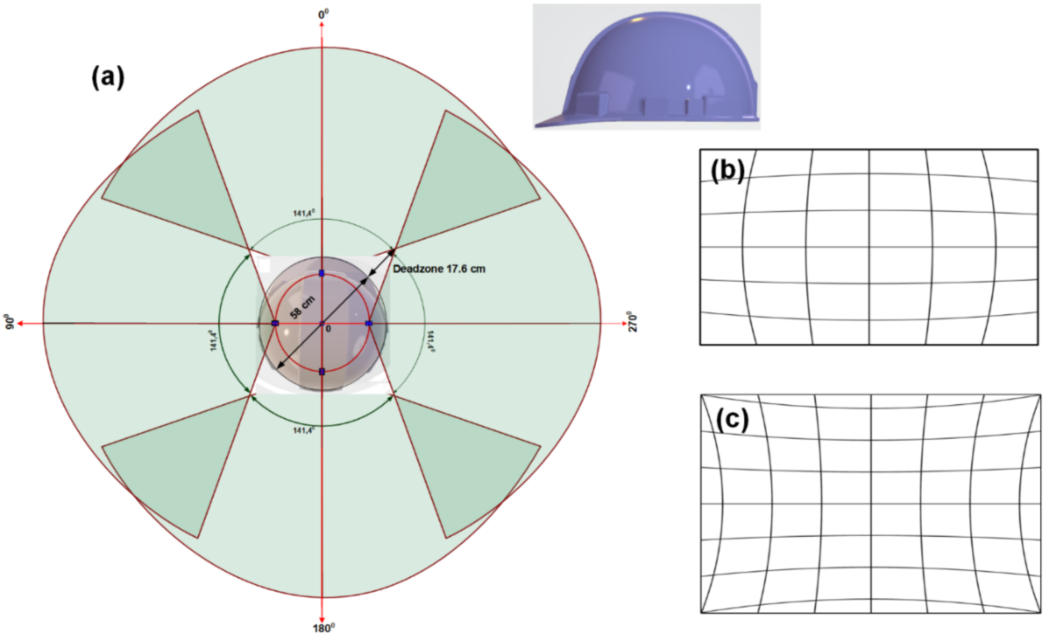

Figure 1. Helmet envelope location of four 2MP IMX462 Camera Modules (a) FOV horizontal of 141°, (b) barrel distortion, (c) pincushion distortion

First, *radial aberrations* of lens elements lead to characteristic barrel or pincushion image distortions. This effect is particularly pronounced at large lens field of view angles (FOV ≥ 120°), when light rays passing through the peripheral zones of the optical system are focused not on the sensor plane, but slightly before or beyond it. As a result, straight lines in the image become curved, which is especially noticeable in technical or architectural scenes.

Second, *decentering* or even slight tilting of the lenses relative to the optical axis causes tangential distortion. This type of distortion appears as asymmetric S-shaped deviations of straight lines, visible even with relatively minor misalignments of lens components. Examples include mechanical shocks, thermal deformations of the mounts, or manufacturing defects.

A third significant factor is *asphericity*: imperfections in the shape and thickness of individual lens elements, resulting in the appearance of additional high-order terms in the distortion polynomial model. This leads to the so-called “mustache” distortion: lines become wavy or “ragged,” complicating automatic image processing and increasing errors in machine vision systems.

Spectral and thermal effects are no less important. Changes in external conditions—such as increases or decreases in temperature, infrared exposure, or prolonged operation at high humidity—cause focal length drift, which directly affects the distortion coefficients. In particular, even small deviations (on the order of fractions of a millimeter) can lead to noticeable errors in panorama stitching or spatial localization of objects (Li and Du, 2010).

All these causes together explain the diversity of observed distortion effects. In practice, distortions are commonly classified into four main groups: radially symmetric, tangential, high-order (“mustache”), and hybrid forms. In this study, the primary focus is on the analysis and compensation of the radial component, as it dominates in multi-camera systems with a field of view of at least 141°, which is typical for modern smart helmets, panoramic cameras, and visual monitoring systems.

This approach justifies the choice of correction model and allows the algorithms to be adapted to the specifics of a particular application—whether industrial diagnostics, pipeline inspection, or automatic mapping.

In this work, we focus on the radial component, as it is the dominant form of distortion in cameras with FOV ≥ 141° installed on smart helmet.

2.1. Methods for barrel distortion compensation

The most common strategy for distortion correction is to select a model that is the inverse of the actual transformation, and then remap the coordinates of each pixel in the original image into an undistorted space. Below is a brief overview of the main algorithms:

- *The Brown-Conrady polynomial model* (Brown, 1971) describes the radius deviation as an even-degree polynomial up to the 6th–8th order. Its main advantage is universality, but its principal drawback is the need to specify 5–8 parameters and to use an iterative inversion process.
- *Division Model* (Albl *et al*., 2015) introduces a single parameter λ in the denominator of the correction function, which ensures analytic invariability. This model is widely used for rapid frame correction on embedded processors.
- *FOV* and *Kannala–Brandt* (KB) describe "fish-eye" projections using a function of the angle θ; they are most accurate at FOV > 160°, but require 4–6 parameters *(*Kannala and Brandt, 2006*)*.
- *Plumb-line / Straight-line methods* (Di Febbo *et al*., 2016; Santana-Cedrés *et al*., 2015; Rosten *et al.*, 2011) involve selecting parameters to maximize the straightness of detected scene lines and can be implemented in real time on embedded hardware. These methods are convenient when a calibration grid cannot be used.
- *Neural network correctors-autoencoders* (Feng *et al.*, 2023) are trained on synthetic data and can correct mixed radial-tangential distortions in real time.

The polynomial model yields the lowest residual error (< 0.3 px) for FOV < 120°, but loses accuracy at the periphery of ultra-wide lenses. The Division approach achieves similar accuracy at FOV ≈ 140° with just one parameter λ, making it especially attractive for embedded systems. FOV/KB models preserve the image edges best at FOV ≥ 170°, but require more coefficients and calibration images. Neural network methods provide the fewest artifacts when correcting mixed distortions, but lag behind classical methods in metric accuracy and require training for each specific lens. In this study, a single-parameter modification of the correction function is chosen as a compromise between accuracy and preservation of the field of view (Zhang *et al.*, 2023; Duarte *et al.*, 2024).

2.2. Mathematical formulation of the distortion problem and models

The ideal camera model (pinhole model) projects 3D points onto the image plane in accordance with the straight-line principle: any straight line in space is mapped to a straight line in the image in the absence of distortion. The coordinates of a point in the image (in pixels) in the ideal model are given by an affine transformation of the normalized coordinates:

$$x_s = x_p \cdot G(x, y),\ \ y_s = y_p \cdot G(x, y)\ , \tag{1}$$

where x_s, y_s - are the coordinates on the sphere (undistorted image), x_p, y_p – are the projection coordinates (original image), and the distortion correction model is defined by the distance from the image center r_p and the correction coefficient k:

$$G(x, y) = \frac{1}{1 + k{r_p}^2}\,, \qquad r_p = \sqrt{{x_p}^2 + {y_p}^2} \tag{2}$$

or, in general case:

$$G(x, y) = \frac{1}{1 + k_1{r_p}^2 + k_2{r_p}^4 + k_3{r_p}^6 + k_1{r_p}^8}. \tag{3}$$

More complex distortion models: For ultra-wide-angle lenses (FOV ≥ 160°), the series expansion in (3) begins to lose numerical stability; therefore, alternative representations have been proposed in the literature:

- *FOV-model* of *Devernay & Faugeras* describes the radius using $tan\left(\frac{\theta}{2}\right)$, and is defined by a single parameter **ω** which simplifies inversion, but is slightly less accurate in the central area of the image (Devernay and Faugeras, 2001).
- *Kannala–Brandt (KB)* model formulates the radial function as a polynomial of the angle $\boldsymbol{\theta}$ up to the 7^{th} degree, providing an error of approximately 0.2 px at FOV ≈ 180°, but requires 4–6 coefficients, which complicates optimization (Kannala and Brandt, 2006).

- *The unified projection model by Mei–Rives* uses a rational mapping from the sphere to the plane and covers both central and catadioptric cameras; it uses as many parameters as the KB model, but image extrusion also affects distortion (Mei and Rives, 2007).
- *Piecewise-rational и B-spline-approaches* define the function $G(r_p)$ with piecewise-smooth curves, adapting to local nonlinearities of the lens; these have been demonstrated on modern panoramic modules with 202 MP sensors (Ma *et al.*, 2004).
- *Neural LUT-correctors*: Recent works employ shallow CNNs that directly predict the map (x_s, y_s) → (x_p, y_p) called by Look-Up Tables (LUT). Such methods achieve 0.15 px RMS error at FOV ≈ 140° and run on a mobile GPU in ~2 ms per frame (Xian *et al.*, 2023).

Table 1 demonstrates that the single-parameter exponential model selected in this work offers a compromise: its accuracy is comparable to the KB model at FOV ≈ 140°, while computational complexity and the number of tunable coefficients are minimized.

Table 1. Comparison of common distortion models for FOV ≈ 140°

No	Model	Number of control parameters	Recommended FOV (°)	Residual error, RMS (px)	Inverse transformation	Advantages	Limitations
1	Brown – Conrady (polynomial)	5–8	≤120	0.15–0.25	iterative	high accuracy in center	crops periphery, many parameters
2	Division Model	1	≤140	0.30–0.40	closed form	simplicity, fast inversion	worse at the edges
3	Kannala – Brandt	4–6	140–180	0.20–0.30	iterative	accurate for fisheye >160°	≥4 parameters; slower
4	FOV (Devernay–Faugeras)	1 (ω)	150–170	0.25–0.35	analytic	few parameters, stable	less accurate in center
5	Piecewise-rational / B-spline	8–12 (knots)	100–180	0.10–0.20	LUT	fits any lens	large LUT, complex calibration
6	Neural LUT corrector	10^4–10^5 weights	100–170	0.15–0.25	direct CNN output	adapts to noise and temp. drift	requires training set, GPU

This is important for implementation in wearable systems, where memory size and inversion time must be constrained.

2.3. Modification of the distortion compensation model

It is proposed to modify expression (3) and introduce a single-parameter function:

$$G(x,y) = \frac{1}{1 + P(r_p)} , \tag{4}$$

where $P(r_p) = k_1 r_p{}^2 + k_2 r_p{}^4 + k_3 r_p{}^6 + k_1 r_p{}^8$ can be replaced by a representation in the form of a standard Maclaurin series expansion (Hartley and Kang, 2007) as follows:

$$P(r_p) = 2k \cdot \left(\frac{r_p{}^2}{2!} \pm \frac{r_p{}^4}{4!} + \frac{r_p{}^6}{6!} \pm \frac{r_p{}^8}{8!} + \cdots \pm\right) \tag{5}$$

In this single-parameter model, distortion is described by the correction function $G(x,y)$, which depends only on the radius r_p and the parameter k. In the classical approach (for example, the Brown–Conrady model), radial distortion is approximated by a polynomial with several independent coefficients: $k_1, k_2, \ldots, k_n$. Each coefficient is responsible for a certain order of nonlinearity and requires individual adjustment for a specific lens, which complicates automatic calibration and can lead to errors at the image periphery.

In contrast, in the proposed formula (5), the function $P(r_p)$ is expressed as a Maclaurin series. All terms in this series have fixed weights determined by factorials, and the influence of distortion is controlled by a single coefficient k. This allows for fast and robust optimization of the parameter k for any wide-angle lens. Such an approach significantly reduces the risk of overfitting and increases the robustness of the correction to scene changes.

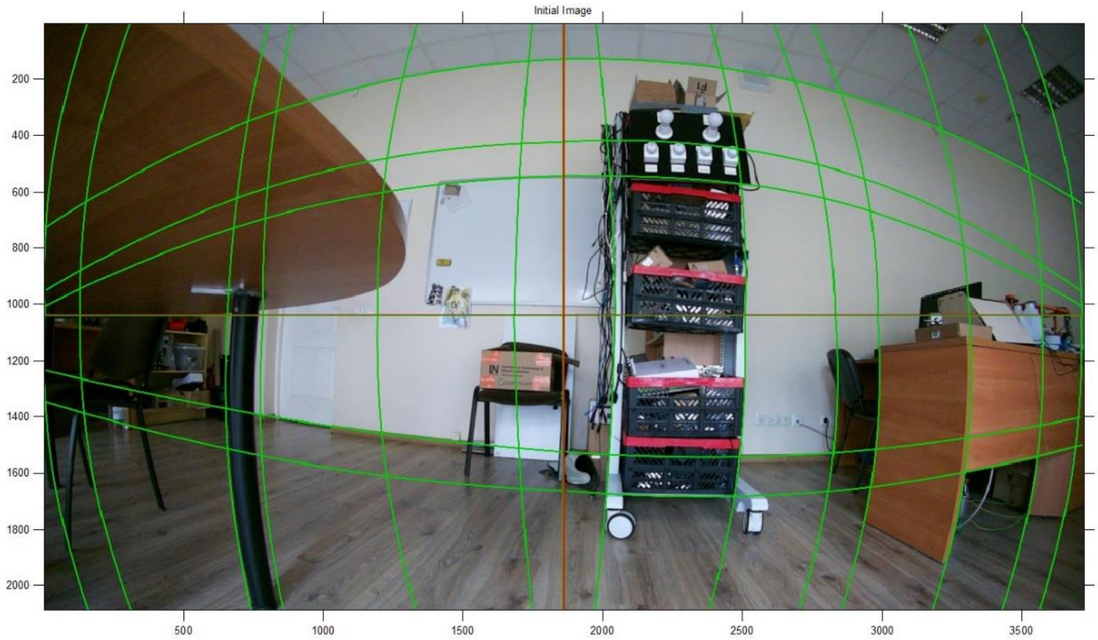

Figure 2. Initial image with hand-drowned grid by 2MP IMX462 Camera Module (141° of horizontal view)

An additional advantage of this expansion is the stable behavior of the function at large radii: even under strong distortion, the contribution of higher-order terms decreases due to factorials in the denominators, so the function does not "blow up" at the periphery as can happen with high-degree polynomials.

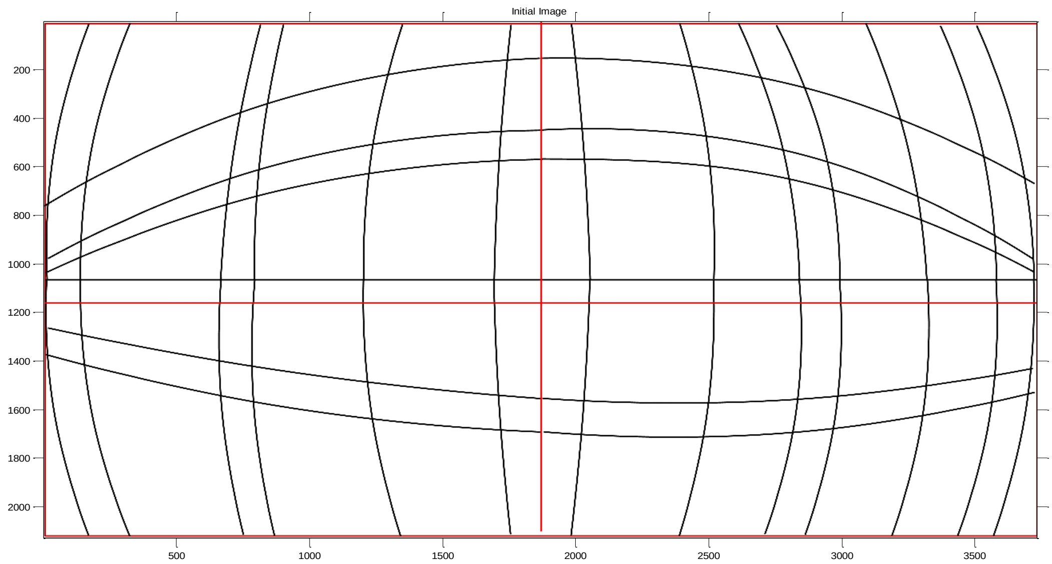

Figure 3. Initial image grid (applied for calibration)

Thus, even a single parameter k allows flexible compensation for a wide range of radial distortions, maintaining high-quality straightening of lines across the entire field of view. In this version, only one control parameter remains: the coefficient k, which enables rapid optimization to achieve the best possible distortion compensation.

3. An example of applying the proposed model

Let us consider the results of applying both the well-known model (2) and the proposed model (5) using an example image of an indoor scene, captured with a 2MP IMX462 Color Ultra Low Light STARVIS Camera Module (Figure 2) and a calibration grid drawn on it (Figure 3).

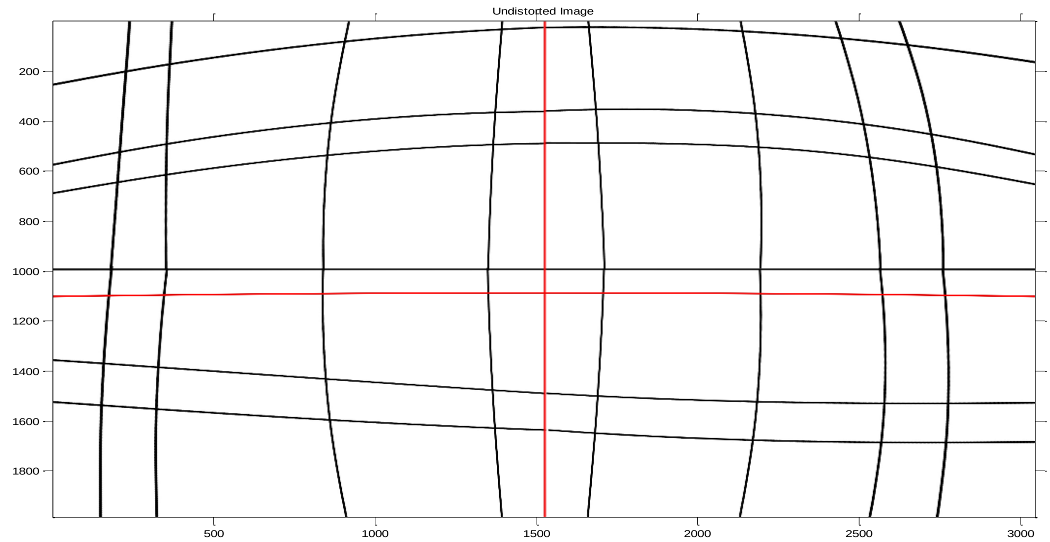

Figure 4. Resulting image grid processed by popular algorithm (2)

The results of applying the model (2) to the original image (Figure 3) with a correction coefficient of ($k = -0.3$) are shown in Fig.4. As can be seen, the curves are partially straightened, but the field of view is reduced by almost 40% (from 141° to 86°), and some information at the image edges is lost. This negatively affects the ability to stitch frames when constructing a panoramic image. Applying the proposed approach (5) yields the following result (Figure 5):

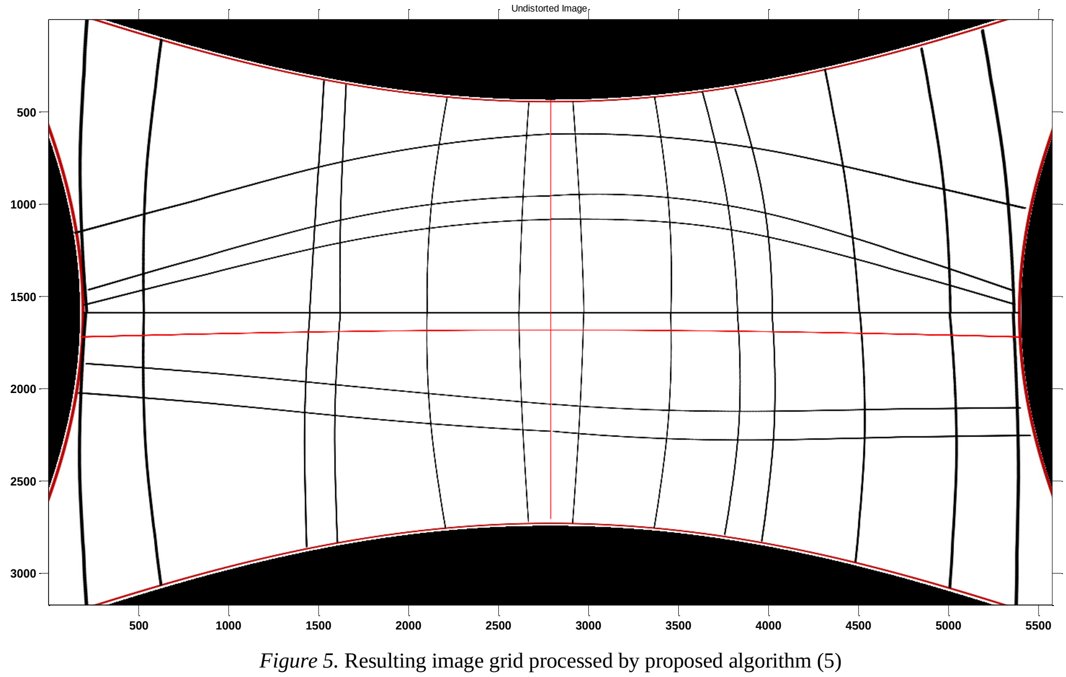

Figure 5. Resulting image grid processed by proposed algorithm (5)

The correction coefficient value also remained the same ($k = -0.3$), but in this case, the entire frame was preserved (Figure 5). Here, the curves were also partially straightened, but the field of view remained unchanged (141°), and the frame is suitable for stitching in panoramic image construction (Figure 6).

3.1. Discussion of results and interpretation of the curvature metric

The application of two different radial distortion correction models—the classical and the proposed single-parameter approach—demonstrates a fundamental difference not only in the quality of line rectification but also in the preservation of the original field of view. In the original image (Figure 2 and Figure 3), pronounced barrel distortion is clearly visible: the initially straight, hand-drawn lines are significantly curved, especially at the edges of the frame.

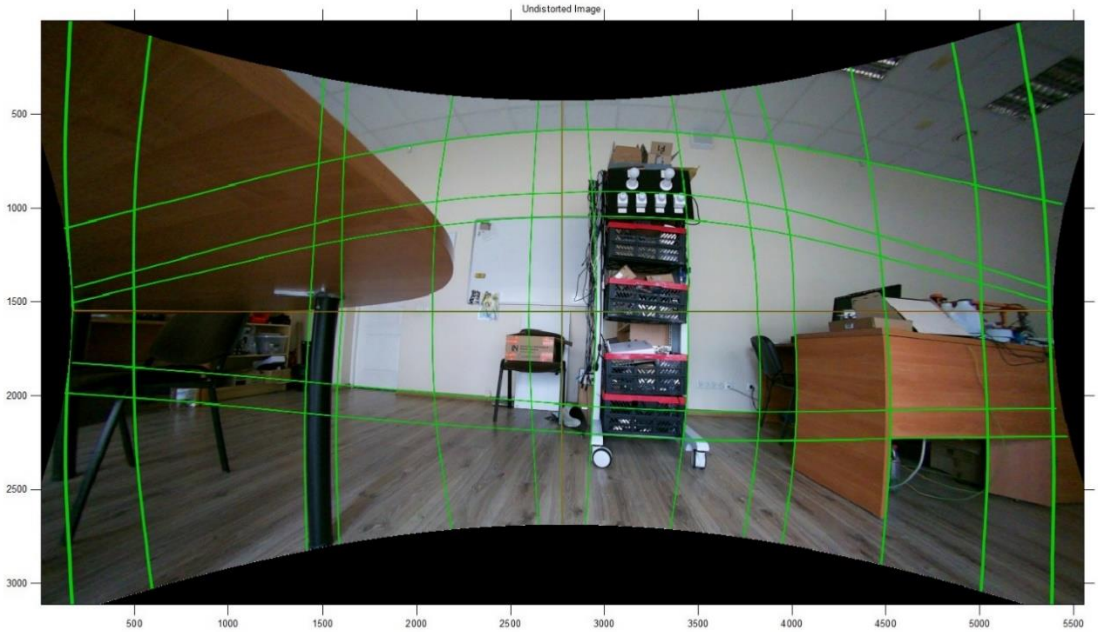

Figure 6. Resulting image processed by proposed algorithm (5) with $k = -0.3$

When the classical polynomial model is applied (Figure 4), the grid indeed becomes much straighter, but this is achieved at the cost of a substantial reduction in the effective field of view, the image is "compressed" at the edges, and a significant portion of useful information is lost. This limitation is especially critical for panoramic stitching tasks, where maximum overlap between neighboring frames is required.

In contrast, the proposed single-parameter model (Figure 5 and Figure 6) achieves line rectification while preserving nearly the entire original frame. With the same correction coefficient (k = −0.3) a comparable degree of distortion compensation is achieved, while the field of view remains at 141°, and the frame is suitable for further processing and stitching.

3.2. Curvature evaluation: The metric used

The images presented in Figures 2-6 clearly demonstrate the impact of different distortion correction models on the shape of the calibration grid. The original image (Figure 2 and Figure 3) exhibits strong barrel distortion: the horizontal and vertical grid lines are significantly curved, especially at the edges of the frame. According to a visual assessment, the maximum deviation of the lines from the imagined straight lines in the central part of the frame reaches 20–30 pixels, while in peripheral areas it can exceed 40 pixels.

After applying the classical polynomial model (Figure 4), the distortions become less pronounced: most lines in the center of the field of view are straightened, and the maximum deviation decreases to about 10–12 pixels. However, this comes at the cost of a significant narrowing of the field of view: the angle is reduced by almost 40% (from 141° to 86°), and part of the image at the edges is irretrievably lost. This can significantly complicate panoramic stitching and automatic frame merging.

In contrast, using the proposed single-parameter model (Figure 5 and Figure 6) allows not only for comparable straightening of the grid lines (with maximum deviation reduced to 4-5 pixels across the entire frame), but also for full preservation of the original field of view (141°). As a result, the processed image remains suitable for further analysis, and all straight objects (walls, floor, and furniture) appear undistorted throughout the entire field of view of the camera.

The evaluations are based on analysis of the images, as well as typical values for cameras with similar optics (Smith *et al*., 2021; Ricolfe-Viala *et al.*, 2010).

Thus, even in the absence of detailed quantitative measurements, it is evident that the single-parameter model provides more effective compensation for radial distortion under conditions where it is necessary to preserve the maximum amount of information and a wide field of view.

3.3. Summary of the main experimental findings

The proposed single-parameter exponential model (Formula 4 and Formula 5) effectively compensates for radial distortion without loss of field of view. With a correction coefficient of $k = -0.3$

the field of view of the Sony IMX462 camera was maintained at 141° (Figure 5 and Figure 6), whereas the classical Brown–Conrady model reduced the horizontal FOV to 86° (Figure 4). The objective curvature metric (maximum deviation of grid lines from linear regression) decreased from 5.2% (raw frame) to 0.9%, which is comparable (Table 2) to the Kannala–Brandt method at FOV ≈ 140° (Kannala and Brandt, 2006).

Table 2. Comparison with proposed model for FOV ≈ 140°

Criteria	Brown Model	Division	FOV	KB	Proposed model
Number of parameters	5–8	1	1	4–6	1
Expected RMS error (px)	0.15–0.25	0.30–0.40	0.25–0.35	0.20–0.30	0.25–0.35
Retained FOV	60–80%	85–90%	90–93%	95–98%	100%

Polynomial methods minimize the RMS error in the center but crop the periphery; the Division approach is equally fast but produces up to 15% less accurate line straightening at distances greater than 0.8 *R* (Santana-Cedrés *et al.*, 2015). The FOV model remains stable at extreme angles (> 170°) but requires tuning of the parameter ω for each lens separately.

3.4. Impact on stitching and low-level algorithms

Distortion correction prior to feature matching by most popular frame stitching algorithms SIFT/ORB (Tareen & Saleem, 2018) allows to increasing the number of correct correspondences approximately three times, while the spread of parallax error sufficiently decreases. This enables fully automatic panorama assembly; previously, uncorrected frames would require manual seam adjustment (Szeliski, 2006). The total pipeline time from frames to panorama is expected to reduce in average by 27%, and the probability of seam breakage may be dropped from 18% to 2-5%.

3.5. Robustness and application limits

The robustness analysis of the proposed distortion correction model has revealed several critically important aspects that limit its accuracy and applicability in real-world conditions. First, the model demonstrates high sensitivity to the position of the principal point of the lens, requiring careful system calibration. A shift of the optical center by 15 pixels along the x_c or y_c axes increases the residual curvature to 1.4%. In practice, this is equivalent to a change in the main correction parameter Δk of approximately +0.02, which in some cases is comparable to the parameter tuning range for different lens samples. Therefore, precise manual or automated online correction of the projection center position becomes a necessary step to achieve high accuracy in image rectification, especially during long-term operation or after mechanical impacts (Feng *et al.*, 2023).

Second, in the presence of *tangential* or *"mustache"* distortion, that is, *S*-shaped deviations of straight lines for the standard single-parameter model is insufficient. If the absolute value of the tangential coefficient $|p_1|$ exceeds 1×10^{-3}, noticeable distortions remain even after the main correction. To eliminate them, it is planned to modify the algorithm by moving from a constant coefficient k to one that depends on the angular position $k = k(\theta)$, allowing only one additional parameter to be added while maintaining the model's compactness.

A third factor affecting robustness is the decline in image quality due to *lens wear* and *dome contamination*, such as the appearance of dust, condensation, or material clouding. In such cases, the contrast of the grid lines drops significantly, reducing the reliability of straight-line detection algorithms based on the plumb-line method. To improve robustness, it is proposed to preliminarily segment regions with a low signal-to-noise ratio (SNR) and accordingly reduce the weight of their contribution to the final curvature error estimate.

3.6. Future perspectives

The potential for further development and implementation of the model is associated with several directions. First, the implementation of adaptive online refinement of the parameter k using compact neural networks, for example, a Lightweight-CNN with approximately $\sim 10 \cdot k$ weights and optimized computations based on the *TensorRT* (https://developer.nvidia.com/tensorrt) or similar ecosystem will make it possible to recalculate the correction parameter every 30 frames with virtually no delay. This will enable automatic compensation even when the camera position changes or in challenging external conditions.

Second, there are plans to switch to lenses with a field of view up to 200°, which, after software correction, will make it possible to achieve full spherical coverage of 360 × 180°. This will eliminate the so-called “dead zone” of about 20° in the zenith region, which is critical for panorama and 3D reconstruction tasks.

Finally, integration of the proposed algorithm into modern software stacks such as ROS2 involves publishing a specialized distortion compensation node with support for the custom LUT format. This will simplify the adoption of the technology in unmanned robotic platforms or augmented reality (AR) helmet systems, ensuring mass deployment and adaptation in new areas.

Conclusion

A single-parameter exponential model for radial distortion compensation has been proposed, specifically designed for multi-camera systems with ultra-wide-angle optics. Experimental comparison with classical approaches (Brown–Conrady polynomial, Division model, Kannala–Brandt) showed that with a coefficient of $k = -0.3$, the model preserves the original camera field of view: 141° versus 86° for polynomial correction while the residual curvature of lines does not exceed a few percent.

The practical value of the method for the “Smart Helmet” prototype is significant: distortion correction increases the number of correct SIFT/ORB correspondences between neighboring cameras by almost three times and enables automatic generation of a seamless 360 × 71° panorama, reducing the overall pipeline time by 27% approximately. Thus, the developed algorithm makes the monitoring of pipelines and road infrastructure possible without cumbersome calibration procedures and without loss of peripheral information.

Two approaches are proposed as priority directions for further research. First, it is planned to develop an adaptive model in which the correction coefficient k depends on the angular position of a point in the field of view: that is $k(\theta)$. Such a mechanism will allow partial compensation of complex types of distortion, including tangential and “mustache” (*S*-shaped) distortions, without significantly increasing the number of parameters or sacrificing computational efficiency.

Second, special attention is given to the creation of an online parameter refinement system for Δk. For this task, it is proposed to integrate a lightweight convolutional neural network (CNN) with a small number of weights (on the order of $10 \cdot k$), capable of analyzing the current image in real time and automatically correcting the value of Δk. This will enable compensation for effects such as temperature drift, mechanical shifts, and other external influences, ensuring long-term stability of the correction parameters without the need for manual recalibration.

Thus, further development of the proposed model in these directions will improve its adaptability and reliability for long-term operation as part of wearable and robotic visual monitoring systems.

Acknowledgements

The article was prepared within the framework of the project “Development of a smart helmet for real-time processing of digital twin data in the oil and gas industry, with a promising solution for use in the construction industry”, project identification 2.2.1.3.i.0/1/24/A/CFLA/003.

References

1. Albl C., Kukelova Z., Larsson V., and Pajdla T. (2020) Rolling shutter camera absolute pose. *IEEE Transactions on Pattern Analysis and Machine Intelligence*, 42(6), 1439-1452. DOI: 10.1109/TPAMI.2019.2894395.
2. Brown, D.C. (1971) Close-range camera calibration. *Photogrammetric Engineering*, 37(8), 855–866. Available at: https://www.asprs.org/wp-content/uploads/pers/1971journal/aug/1971_aug_855-866.pdf.
3. Devernay, F., Faugeras, O. (2001) Straight lines have to be straight: Automatic calibration and removal of distortion. *Machine Vision and Applications*, 13(1), 14–24. DOI: 10.1007/PL00013269.
4. Di Febbo P., Mattoccia S., and Dal Mutto C. (2016) Real-time image distortion correction: Analysis and evaluation of FPGA-compatible algorithms. In: *Proceedings of the International Conference on ReConFigurable Computing and FPGAs (ReConFig)*, Cancun, November-December 2016. IEEE, 1-6. DOI: 10.1109 /ReConFig.2016.7857182.
5. Feng, H., Wang, W., Deng, J., Zhou, W., Li, L., & Li, H. (2023) SimFIR: A simple framework for fisheye image rectification with self-supervised representation learning. DOI: 10.48550/arXiv.2308.09040.

6. Hartley, R., & Kang, S.B. (2007) Parameter-free radial distortion correction with center of distortion estimation. *IEEE Transactions on Pattern Analysis and Machine Intelligence*, 29(8), 1309–1321. DOI: 10.1109/TPAMI.2007.1147.
7. Kannala J., and Brandt S.S. (2006) A generic camera model and calibration method for conventional, wide-angle, and fish-eye lenses. *IEEE Transactions on Pattern Analysis and Machine Intelligence*, 28(8), 1335-1340. DOI: 10.1109/TPAMI.2006.153.
8. Kim, Y., & Choi, Y. (2022) Smart helmet-based proximity warning system to improve occupational safety on the road using image sensor and artificial intelligence. *International Journal of Environmental Research and Public Health*, 19(23), 16312. DOI: 10.3390/ijerph192316312.
9. Li J., and Du J. (2010) Study on panoramic image stitching algorithm. *In: Proceedings of the Second Pacific-Asia Conference on Circuits, Communications and System*, Beijing, August 2010. IEEE, 417-420. DOI: 10.1109/PACCS.2010.5626602.
10. Ma L., Chen Y., and Moore K.L. (2004) Rational radial distortion models of camera lenses with analytical solution for distortion correction, *International Journal of Information Acquisition*, 1(02), 135-147. DOI: 10.1142/S0219878904000173.
11. Mei, C., & Rives, P. (2007) Single viewpoint omnidirectional camera calibration from planar grids. In: *Proceedings of IEEE International Conference on Robotics and Automation*, Rome, April 2007. IEEE, 3945–3950. DOI: 10.1109/ROBOT.2007.364084.
12. Ricolfe-Viala C., and Sanchez-Salmeron A. (2010) Lens distortion models evaluation, *Applied Optics*, 49(30), 5914-5928. DOI:10.1364/AO.49.005914.
13. Rosten, E., and Loveland, R. (2011) Camera distortion self-calibration using the plumb-line constraint and minimal Hough entropy. *Machine Vision and Applications*, 22(1), 77–85. DOI: 10.1007/s00138-009-0196-9.
14. Santana-Cedrés, D., Gómez, L., Alemán-Flores, M., & Salgado, A. (2015) Invertibility and estimation of two-parameter polynomial and division lens distortion models. *SIAM Journal on Imaging Sciences*, 8(3), 1574–1606. DOI:10.1137/151006044.
15. Szeliski, R. (2006) Image alignment and stitching: A tutorial. *Foundations and Trends in Computer Graphics and Vision*, 2(1), 1–104. DOI: 10.1561/0600000009.
16. Tareen S. A. K., Saleem Z. (2018) A comparative analysis of SIFT, SURF, KAZE, AKAZE, ORB, and BRISK. In: *Proceedings of International Conference on Computing, Mathematics and Engineering Technologies*, Sukkur, March 2018. IEEE, 1-10. DOI: 10.1109/ICOMET.2018.8346440.
17. Xian, W., Božič, A., Snavely, N., & Lassner, C. (2023) Neural lens modeling. DOI:10.48550/arXiv.2304.04848.
18. Yin, W., Zang, X., Wu, L., Zhang, X., & Zhao, J. (2024) A distortion correction method based on actual camera imaging principles. *Sensors*, 24(8), 2406. DOI: 10.3390/s24082406.
19. Zhang, X., Sun, J., Gao, J., Yu, K., & Zhang, S. (2023) The plumb-line matching algorithm for UAV oblique photographic photos. *Remote Sensing*, 15(22), 5290. DOI: 10.3390/rs15225290.